Modeling Shockwaves Generated by Explosive Volcanic Eruptions

E. F. Medici,[1] J. S. Allen,[1] and G. P. Waite[2]

[1] Department of Mechanical Engineering - Engineering Mechanics, Michigan Technological University, Houghton, Michigan, USA.

[2] Department Geological and Mining Engineering and Science, Michigan Technological University, Houghton, Michigan, USA.

Keywords: Shock waves, Shock Tube, Explosive Eruption

Key point: Shock wave model based on infrasound measurements to assess eruption size.

---

[1]Corresponding Author: E. F. Medici,
Department of Mechanical Engineering -
Engineering Mechanics, Michigan
Technological University, 1400 Townsend
Dr., Houghton, Michigan 49931, USA.

Atmospheric shock waves induced by explosive volcanic eruptions can provide valuable information about eruption characteristics. Shock waves are manifest as pressure-density gradients that can be remotely observed with relatively little noise. Field measurements of expanding shock waves can be directly recorded by pressure transducers or imaged under the proper illumination and atmospheric conditions. In this paper, an open-ended shock tube was used to generate weak shock waves in the laboratory that are representative of explosive volcanic eruptions. They indicate that strong shock wave theory can still be used for modeling moderate volcanic eruptions. Based on that finding, we use strong shock theory to estimate sudden the explosive energy released from several explosive eruptions. Our energy calculations are well correlated with total energy estimates derived from plume height or erupted mass.

1. Introduction

Explosive volcanic eruptions have been the focus of many studies ranging from field measurements to scale laboratory models mimicking the dynamics of eruptions. Laboratory experiments allow for studies of isolated aspects of an eruption in a controlled environment. One characteristic of explosive volcanoes is the formation of atmospheric shock waves. These shock waves can travel significant distances from the volcanic vent, as shown by *Morrissey and Chouet* [1997], carrying important information about the dynamics of the eruption. When energy is suddenly released into the atmosphere, a sound wave is generated. If the energy released is large enough, such as in some volcanic eruptions, a shock wave is generated instead. A shock wave differs from a sound wave in that it is traveling faster than the speed of sound. As the shock wave propagates, it gradually losses speed until the velocity is equal to the speed of sound, at which point it becomes a sound wave. In explosive volcanism (vulcanian to plinian), generation of an atmospheric shock wave is expected.

Shock waves in volcanoes have been reported in a limited number of eruptions [*Morrissey and Mastin*, 2000]. This is mostly because they can be visually observed only under certain specific environmental conditions. Although shock waves have not been reported in every explosive eruption, weak shock waves may occur frequently. High pressure measurements near explosive volcanoes may be indicative of the generation of shock waves. However, shock waves typically transition to sonic waves shortly after generation. Surface topography may also reflect the shock wave, giving inaccurate measurements from ground-based sensing [*Wohletz and Valentine*, 1990].

There has been some limited work on shock waves generated by volcanic eruptions. Within the volcanic conduit, supersonic flow produced by decompression has been analytically modeled [*Woods*, 1995], including the effect of a diffusing vent [*Woods and Bower*, 1995], but the formation of an atmospheric shock wave was not considered. *Morrissey and Chouet* [1997] developed a numerical model of shock wave propagation in the atmosphere generated during a volcanic eruption, but this model does not include the effect of the geometry of the vent, nor the effect of topography. *Saito and Takayama* [2005] performed a series of numerical simulations of a shock waves generated during a volcanic eruption including the very specific topography of Mt. Fuji. However, those simulations were site specific and can not be generalized. There are also limited studies on the hazards of volcanic atmospheric shock wave (e.g., *Saito et al.* [2001]), which have resulted in significant damage to structures during eruptions of Asama in 2004 and Sakurajima in the 1980s [*Yokoo et al.*, 2006; *Yokoo and Ishihara*, 2007].

Experiments scaled to volcanic eruptions are scarce. Planar or normal shock waves generated during compression-decompression within a shock tube can not be directly compared with the spherical expanding shock waves propagating into the atmosphere [*Chojnicki et al.*, 2006]. Experiments conducted with small (˜MJ) explosive sources show that the depth of the source, as well as the vent geometry, control the energy in the blast wave and the velocity of ejected particles [*Taddeucci et al.*, 2013; *Goto et al.*, 2001].

In an atmospheric shock wave, the speed of the wave is proportional to the intensity of the source that generated it, in this case the volcanic eruption. That is not the case for sonic waves, in which the propagation speed is equal to the speed of sound in the

propagating media. Yet, a good correlation has been shown between the acoustic energy, obtained by integrating of the infrasound signal of the eruption, and the plume heights [*Garcés et al.*, 2008; *Dabrowa et al.*, 2011; *Fee and Matoza*, 2013; *Caplan-Auerbach et al.*, 2010]. However, the calculations of the acoustic energy, which is entirely based on the spherical expansion of a sound wave, might underestimate the plume height when a shock are present, as suggested by *Caplan-Auerbach et al.* [2010].

In this paper, the proportionality between shock wave speed and detonation energy is used to model the peak pressure at the volcanic vent and the sudden energy released by the eruption. Total energy released by a volcanic eruption is typically estimated from the mass of erupted material, relating thermal energy release to erupted volume or by correlations with the plume height [*Morton et al.*, 1956]. The use of a shock wave model allows an independent estimate of the sudden energy release, although the energy associated with long-duration eruptions will be underestimated. A potential advantage of using a shock wave model to estimate the sudden eruption energy released, intensity, and other aspects of the eruption dynamics is that field measurements can be safely made remotely. Another advantage is that the measurement of the shock wave is relatively free of noise as compared with other remote sensing data. Similar potential monitoring advantages have been identified by using infrasound measurements from the International Monitoring System (IMS) [*Garcés et al.*, 2008; *Dabrowa et al.*, 2011; *Fee and Matoza*, 2013]

In this paper a simplified approach is proposed to estimate the initial impulsive energy source of a explosive eruption based on the shock wave it generates. A modified shock

tube is used to generate spherical shock waves from which the explosive power, shock wave speed of propagation, and pressure ratios are measured and compared to the predictions from shock wave theory. The shock tube experiment conditions are scaled to simulate conditions occurring during a volcanic eruption. The value of the initial pressure as well as the size of the shock tube is scaled from comparative volcanic eruptions.

2. Experimental Modeling

A Split-Hopkinson pressure bar test gun was used to generate the shock waves. This shock tube consists of a cylindrical high pressure, or driver, section 0.73 m in length and 0.14 m in diameter (Figure 1). The driven section is 0.0254 m in diameter and 1.2 m in length, while 0.6 m of that length resides inside the driver section.

The driver section is filled with nitrogen at different test pressures. The driven section is open to the atmosphere and filled with air at room temperature and pressure of 18^oC and 101.1 kPa, respectively. The driver section is first pressurized by opening the filling valve, filling the buffer chamber and subsequently the driver section though a small leakage between the piston and the cylinder (green stream lines in Figure 1). Once the buffer chamber and driver section are filled, the filling valve is closed. To trigger the shock tube, the firing valve is suddenly opened evacuating all the nitrogen from the buffer chamber. With the buffer chamber at lower pressure than the driver section, a rapid backward motion of the piston occurs. The nitrogen stored in the driver section then expands into the driven section creating a shock wave (red stream lines in Figure 1).

The shock wave is visualized using the shadowgraph technique. The lenses used in the shadowgraph arrangement are 0.28 m in diameter 0.5 m in focal length. High speed

visualization was achieved using a Photron APX-RS CMOS camera capable of 3000 fps at full-field and up to 250,000 fps at reduced-field. A Kulite XLT-123b-190 pressure transducer is located at 0.019 m from the end of the driven section. The signal from this pressure transducer is used to trigger the video camera. The signal from the transducer was acquired using a NI PCI-6143 data acquisition board at a sampling period of 4 μs.

3. Experimental Results

The evolution of the shock waves generated in our experiments can be divided into two main stages: planar or normal shock wave propagation in the driven section, followed by a spherical expansion into the open atmosphere at the end of the driven section. The shock wave travels through the driven section as a flat disk. Since the driven section has a constant diameter it does not allow for expansion or contraction of the shock wave as in a regular close end shock tube *Gaydon and Hurle* [1963]. For a normal shock wave traveling inside the driven section, the pressure ratio between the driver pressure P_4 (load shock tube pressure) and the atmospheric pressure P_1 can be expressed in terms of the non-dimensional wave speed or Mach number, M:

$$\frac{P_4}{P_1} = \frac{2\gamma M^2 - (\gamma - 1)}{\gamma + 1} \left[1 - \frac{\gamma - 1}{\gamma + 1} \left(M - \frac{1}{M} \right) \right] \tag{1}$$

where the Mach number is defined as $M = \sqrt{\gamma RT/m}$, where γ is the heat capacity ratio, R is the universal gas constant, T is the local temperature, and m is the molecular mass. The pressure ratio across the shock wave, P_2/P_1 for any shock wave, normal or spherical, can be also expressed in terms of the Mach number, using the Rankine-Hugoniot relationship

[*Shapiro*, 1953]:

$$\frac{P_2}{P_1} = \frac{2\gamma M^2 - (\gamma - 1)}{\gamma + 1} \tag{2}$$

The unknown pressure P_2 and the Mach number, M, can be solved from equations 1 and 2 for the normal shock waves traveling inside the driven section at a known initial driver pressure P_4.

Three tests were performed using nitrogen ($\gamma = 1.4$) at driver test pressures of 8100, 6890, and 5170 kPa. Theoretical pressure jumps, P_2/P_1, of 610, 576, and 520 kPa, and reference Mach numbers of 2.3, 2.24, and 2.14 were obtained, respectively. At the end of the driver section, the shock waves expanded spherically into the atmosphere. The pressure at the exit of the driven section is used as triggering signal for the video imaging. A sequence of 15 to 20 images were taken after a pressure jump was detected at the exit of the driven section. Images were captured at 75,000 fps using the shadowgraph technique. The wave speed was calculated for every pair of adjacent images. The maximum speed is obtained at the initial stage of the expansion and quickly decays to a sound wave (Mach equal to 1). The speed and the relative position from the end of the driven section was calculated between every recorded frame.

Expanding spherical shock waves have been the subject of many studies, especially in artificial explosion applications. In those studies, the intensity of the explosion is large enough to assume that the density change across the shock wave is independent of the pressure ratio across the wave. These are known as strong shock waves [*Shapiro*, 1953]. For this assumption to be valid, the pressure ratio across the shock wave must exceed 50 or Mach larger than 7.6. However, when studying shock waves generated by volcanoes, the

Mach number could be much smaller then 7.6 for smaller eruptions such as the eruptions shown in Table 1. It is necessary then, to determine whether the strong shock wave assumptions are valid for weaker volcanic shock waves.

A scaling of the parameters involved in the generation and expansion of a strong shock wave will produce a relationship between wave speed, time and position [*Sedov*, 1993]:

$$r_d = (Ev_0)^{1/5} t_d^{2/5} \tag{3}$$

$$a_d = \frac{2}{5}(Ev_0)^{1/5} t_d^{-3/5} \tag{4}$$

where r_d and a_d are the position and the wave speed from the detonation point, respectively, t_d is the time since detonation, E is the specific energy accumulated before the detonation, and v_0 is the specific volume of the compressed gas.

Figure 2 shows a comparison of the dimensionless shock wave velocity, Mach number, and position for every experiment (discrete points) and the theoretical prediction based on the strong shock wave approximation from equations 3 and 4. As expected, the strong shock wave theory over predicts experimental weak shock wave speed. For weak shock waves, the power of the energy and time coefficients in equations 3 and 4 are expected to change. A study of the proper fitting power for these weak shock waves will require further studies and is beyond the scope of this paper. However, the comparison of experimental measurements against the scaling of the strong shock wave demonstrate the applicability of the strong shock wave theory despite the presented limitations. This also implies that the strong shock wave scaling can be used as a starting point for modeling weak shock waves generated by volcanic eruptions.

4. Modeling Shocks Induced by Volcanic Eruptions

A spherical pressure wave propagating in the atmosphere normally decays with the inverse of the traveled distance, neglecting atmospheric absorption, due to geometrical spreading. It is a common practice in volcanology to estimate the pressure at a fixed distance from the vent (1 m or 1 km) using recordings made at various distances. This reduced pressure estimate allows for comparison of pressure records from different volcanic eruptions. The reference distance could be larger or smaller; a larger distance will be only representative of the sound wave, not the short-lived shock wave. Using that inverse proportionality of the measured pressure from a sensing station within a few km of the vent, the reference peak pressure at the vent can be calculated as:

$$P_k = \frac{P_m r_m}{r_k} \tag{5}$$

where P_m is the measured pressure, r_m is the distance from the vent of the volcano where P_m is measured, P_k is the peak pressure at the reduced distance, and r_k is the reduced or reference distance at which P_k is calculated. Note that the pressures used in equation 5 are gauge pressures (pressure measured relative to the atmospheric pressure) while absolute pressures are used in any other equation.

The inverse proportionality model can be used for modeling the pressure decay of sound waves or weak shock waves. This procedure might not be adequate for modeling strong supersonic waves since it neglects any energy dissipation due to atmospheric absorption mechanism which could be significant in strong shock waves. However, most volcanic eruptions are in the range of weak shock waves. As shown in the comparison between the scaling and experiments, the strong shock wave model can still be used in weak shock

waves, but it will not be a suitable model for waves that have decayed to sonic speeds. For that reason it is convenient to identify when the transition between supersonic and sonic will occur. Two new quantities, the transition distance, r_t, and the transition pressure, P_t, are defined as the distance and pressure at the transition between sonic and supersonic flow. Free from any interference or obstacle, the transition will occur just above Mach number of 1. We use a transition Mach number, M_t, in the range between 1.005 and 1.015. The pressure in front of the shock wave is the atmospheric pressure, so the transition pressure can be calculated as $P_t = k_t P_{atm}$, where k_t is the pressure ratio obtained using equation 2 for that given transition Mach number. In this case a k_t between 1.023 and 1.047 was obtained. The transition distance r_t can then be solved from equation 5 in terms of P_m as:

$$r_t = \frac{P_m r_m}{(k_t - 1)P_{atm}} \tag{6}$$

The energy that generated the shock wave during the eruption, E_s, can be calculated taking advantage of the pressure versus distance approximation for strong shock waves developed by *Taylor* [1950]. The energy released by the eruption will power a shock wave that will decay into sonic wave at approximately the distance, r_t. Since this is the maximum distance that a shock front can travel for a given initial detonation energy, the energy released can be obtained in terms r_t and P_t or in terms of r_m and P_m using equation 6:

$$E_s = \frac{P_t r_t^3}{0.155} = \frac{(P_m r_m)^3 k_t}{0.155(k_t - 1)^3 P_{atm}^2} \tag{7}$$

Only a few field measurements of pressure waves, potentially shock waves, generated by volcanoes have been reported. Examples include eruptions at Sakurajima [*Yokoo et al.*,

2006; *Yokoo and Ishihara*, 2007], Ngauruhoe [*Nairn*, 1976], Eyjafjallajökull [*Ripepe et al.*, 2013], and Augustine [*Caplan-Auerbach et al.*, 2010]. Table 1, columns 2, 3 and 4 shows the measured pressure at the sensing station, the distance from the station to the vent, and the maximum plume height, respectively, for seven eruptions. Despite the fact that these eruptions have different eruption styles and durations, we can compare the total eruption energy to that estimated from remotely-detected pressure data using the shock wave theory. High values on the infrasound measurements are indicative of a potential shock wave formed at the early stage of the eruption as noticed by *Caplan-Auerbach et al.* [2010]. It is important to note that independently of the eruption dynamics, a sudden release of highly compressed flow into the atmosphere will induce a shock wave as indicated by the scaled laboratory experiments. The same does not apply to the flow evolution following the sudden impulsive event which will largely depend on the eruption dynamics.

Using values from Table 1 in equations 5, 6, and 7; the peak pressure P_k, transition distance r_t, initial Mach number M, and energy released during the shock wave formation E_s, were calculated for the reported pressure measurements near volcanic eruptions as shown in Table 1. The peak pressure is calculated using a reduced distance of 1 m and the initial reference Mach number is solved from equation 2 using the calculated peak pressure. An average atmospheric pressure of 85 kPa (average atmospheric pressure at 1100m elevation) was assumed for all the eruptions analyzed. The transition distance and the energy released are expressed in terms of an average value with an uncertainty due to the expected range in the Mach number, 1.005 to 1.015, at which the transition

between supersonic and sonic might occur. The relatively small uncertainty of 0.5% in the transitional Mach number has a significant effect in the uncertainty of the location of the transition region, 20%, as well as in the energy released, 50%.

The energy calculations summarized in Table 1 column 8 can be compared with the total energy released during the eruption using the correlation between plume height, H, and released thermal energy proposed by *Morton et al.* [1956]:

$$E_b = \left(\frac{H}{1.87}\right)^4 \tag{8}$$

The thermal energy release estimated using equation 8 is representative of the total energy released over the duration of the eruption, while the energy predicted by the shock wave theory is only an estimate of the impulsive energy released during a short period of time. However, a good correlation can be drawn between both quantities.

The energy range calculations presented in Table 1 column 8 are representative of a single, and the largest, event taking place during the eruption. An eruption may consist of a single blast, a series of blasts, or a sustained release energetic enough to produce continuous shocks [*Fee et al.*, 2001]. In addition, a significant amount of energy can be released without producing a shock. Therefore our estimates based on a single shock will underestimate the total energy of the eruption.

In many eruptions the pressure measurements are not available, but instead video imaging of the spherical expanding shock waves have been recorded. In those cases, the peak pressure P_k, energy released by the eruption E, and the initial Mach number can be calculated from the images using the scaling for strong shock waves. As an example, we analyzed video of a small explosive eruption from Mt. Sakurajima's Showa crater at

approximately 1:00 UTC on 30 January 2011. The shock wave positions for 0.2 seconds duration are shown in Figure 3. The shock wave speed between each recorded frame was calculated using a method similar to that proposed by *Yokoo et al.* [2006] and *Yokoo and Ishihara* [2007]. A small region of the imaged area has enough contrast to detect the advancing of the shock wave, as shown in the area of interest highlighted in Figure 3, and only the initial stage of the shock wave has been imaged. Given this limitation, a negligible shock wave speed decay in time was observed. To minimize the error in the calculations, the shock wave velocity for every frame was plotted with time and a linear regression (Figure 4) was used to calculate a speed of 460 m/s. Assuming the speed of sound at 1100 m elevation equal to 335 m/s, a Mach number of 1.37 was obtained. Substituting this value of Mach number into equation 2, yields a pressure ratio of 1.7. Assuming again an atmospheric pressure value of 85 kPa at 1100 m elevation, a pressure behind the shock wave of 172 kPa was obtained. The energy can be now calculated though two different procedures: using equation 7 in combination with the calculated pressure of 172 kPa at an approximate distance from the vent of 100 m (distance form the vent surface to the first detected pixel intensity change due to the advancing of the shock wave); or using equation 3 in combination with the wave speed versus time from Figure 4. Both methods predict an energy released of approximately $1.1 \cdot 10^9$ J. Using the observed plume height of 650 m a total energy released of $1.46 \cdot 10^{10}$ J was obtained using equation (8). It is importance to note that plume reached the elevation of 650 m a few seconds after the eruption implying that there was a large kinetic energy component rather than strictly

buoyancy-driven rise. Nevertheless, this relatively small plume height is indicative of the small scale eruption.

5. Conclusions

The pressure wave generated during an explosive volcanic eruption can be used to estimate the sudden impulsive energy released by the eruption. An open-ended shock tube was used to generate small-scale shock waves representative of a volcanic eruption. Using high-speed imaging, the shock wave speed and position were measured and the results were compared against the strong shock wave theory. The experimental evidence suggests that strong shock wave theory may still be used as a first approximation for modeling weak shock waves induced by explosive volcanoes. However, a more detailed study and scaling of weak shock waves is needed.

In nature, shock waves manifest as pressure-density waves, which can be recorded using pressure transducers or imaged during daylight if atmospheric conditions are favorable. Either type of measurement can provide the shock wave speed and the reduced peak pressure through the Rankine-Hugoniot relationships. We have extended our open-ended shock tube work to volcanic eruptions using pressure measurements from different explosive volcanoes around the world and the video recording of Mt. Sakurajima. By using strong shock theory, we can estimate the energy release associated with the shock-waves generated during these eruptions and compare them to other estimates of eruption energy.

While shock-wave based estimates do not account for the total energy released during sustained eruptions, they do provide an order of magnitude estimate of eruption energy when compared to estimates made from eruption mass and/or plume height. Because

pressure data can be collected in real time, this method may provide a basis for improved early warning of eruption hazard.

Acknowledgments.

We are grateful to James Reynolds for the video of Sakurijima, and to Rudiger Escobar Wolf for enlightening discussions related to this work. Support was provided by the National Science Foundation (EAR-1250153).

References

Caplan-Auerbach J., A. Bellesiles, and J. K. Fernandes (2010), Estimates of eruption velocity and plume height from infrasonic recordings of the 2006 eruption of Augustine Volcano, Alaska. *J. Volcanol. Geotherm. Res.*, *189*(1), 12–18.

Chojnicki K., A. B. Clarke, and J. C. Phillips (2006), A shock-tube investigation of the dynamics of gas-particle mixtures: Implications for explosive volcanic eruptions. *Geophys. Res. Lett.*, *33*(15), L15309.

Dabrowa A. L., D. N. Green, A. C. Rust, and J. C. Phillips (2011), A global study of volcanic infrasound characteristics and the potential for long-range monitoring. *Earth Planet. Sci. Lett.*, *310*(3), 369–379.

Fee, D., R. S. Matoza, K. L. Gee, T. B. Neilsen, and D. E. Ogden (2013), Infrasonic crackle and supersonic jet noise from the eruption of Nabro Volcano, Eritrea, *Geophys. Res. Lett.*, *40*, 41994203, doi:10.1002/grl.50827.

Fee D., R. S Matoza (2013), An overview of volcano infrasound: From Hawaiian to plinian, local to global. *J. Volcanol. Geotherm. Res.*, *249*, 123–139.

Garcés M., D. Fee, A. Steffke, D. McCormack, R. Servranckx, H. Bass, C. Hetzer, M. Hedlin, R. Matoza, P. Yepes, and P. Ramon (2008), Capturing the acoustic fingerprint of stratospheric ash injection. *Eos, Trans. AGU*, *89*(40), 377–378.

Gaydon A. G., and I. R. Hurle I. R. (1963), *The shock tube in high-temperature chemical physics*, Chapman and Hall London.

Goto, A., H. Taniguchi, M. Yoshida, T. Ohba, H. Oshima, (2011), Effects of explosion energy and depth to the formation of blast wave and crater: Field Explosion Experiment for the understanding of volcanic explosion, *Geophys. Res. Lett.*, *28*(22), (2001).

Morrissey M. M., and L. G. Mastin (2000), Encyclopedia of Volcanoes, *Vulcanian Eruptions*, 463–476. Academic Press.

Morrissey M. M., and B. Chouet (1997), Burst conditions of explosive volcanic eruptions recorded on microbarographs. *Science*, *275*(5304), 1290.

Morton B. R., G. Taylor, and J. S. Turner (1956), Turbulent gravitational convection from maintained and instantaneous sources. *Proc. R. Soc. of London, Ser. A*, *234*(1196), 1–23.

Nairn I. A. (1976), Atmospheric shock waves and condensation clouds from Ngauruhoe explosive eruptions. *Nature*, *259*, 190-192.

Nairn I. A., and S. Self (1978), Explosive eruptions and pyroclastic avalanches from Ngauruhoe in February 1975. *J. Volcanol. Geotherm. Res.*, *3*(1), 39–602.

Pyle D. M. (2000), Encyclopedia of Volcanoes, *Size of Volcanic Eruptions*, 263–269, Academic Press.

Ripepe M., C. Bonadonna, A. Folch, D. Delle Donne, G. Lacanna, E. Marchetti, and A Höskuldsson (2013), Ash-plume dynamics and eruption source parameters by infrasound and thermal imagery: The 2010 Eyjafjallajökull eruption. *Earth Planet. Sci. Lett.*, *366* 112–121.

Saito T., and K. Takayama (2005), Applying shock-wave research to volcanology. *Comput. Sci. & Eng.*, *7*(1), 30–35.

Saito T., T. Eguchi, K. Takayama, and H. Taniguchi (2001), Hazard predictions for volcanic explosions. *J. Volcanol. Geotherm. Res.*, *106*, 35–51.

Sedov L. (1993), *Similarity and Dimensional Methods in Mechanics*, CRC Press.

Shapiro A. (1953), *The Dynamics and Thermodynamics of Compressible Fluid Flow, Vol. 1*, Ronald Press, New York.

Taddeucci J., G. A. Valentine, I. Sonder, J. D. L. White, P-S Ross, and P. Scarlato (2013), The effect of pre-existing craters on the initial development of explosive volcanic eruptions: An experimental investigation, *Geophys. Res. Lett.*, *40*(3), 507–510 (2013).

Taylor G. I. (1950), The formation of a blast wave by a very intense explosion. I. Theoretical discussion. *Proc. R. Soc. of London, Ser. A*, *201*, 159–174.

Wohletz K., and G. Valentine (1990), Magma Transport and Storage, *Computer simulations of explosive volcanic eruptions*, 113–135, Wiley, New York.

Woods A. (1995), A model of vulcanian explosions. *Nuclear Engineering and Design*, *155*(1-2), 345–357.

Woods A., and S. Bower (1995), The decompression of volcanic jets in a crater during explosive volcanic eruptions. *Earth Planet. Sci. Lett.*, *131*(3-4), 189–205.

Yokoo A.,and K. Ishihara (2007), Analysis of pressure waves observed in Sakurajima eruption movies. *Earth, Planets, and Space*, *59*(3), 177–181.

Yokoo A., M. Ichihara, A. Goto, and H. Taniguchi (2006), Atmospheric pressure waves in the field of volcanology. *Shock Waves*, *15*, 295–300.

Table 1. Peak pressure P_k, and initial Mach number, and shock wave energy E_s, and total thermal energy E_b calculated using reported pressures measurements and plume heights for some explosive volcanic eruptions.

Eruption	P_m [Pa] (gauge)	r_m [km]	H [km]	P_k [kPa] (abs.)	r_t [m]	M	E_s [J]	E_b [J]
Sakurajima, 1982[1]	140	2.7	-	463	157 ± 31	2.19	$2.4 \pm 1.3 \cdot 10^{12}$	-
Sakurajima, 1987[1]	320	2.7	-	949	360 ± 72	3.11	$2.9 \pm 1.6 \cdot 10^{13}$	-
Sakurajima, 2011 (Video)	-	-	0.65	-	-	1.37	$1.1 \cdot 10^{9}$	$1.46 \cdot 10^{10}$
Ngauruhoe, 1975[2]	240	8.6	11	2235	898 ± 180	4.76	$4.5 \pm 2.4 \cdot 10^{14}$	$1.19 \cdot 10^{15}$
Eyjafjallajökull, 2010[3]	105	8.3	8	956	364 ± 73	3.12	$3.0 \pm 1.6 \cdot 10^{13}$	$3.34 \cdot 10^{14}$
Augustine (Jan 11), 2006[4]	96	3.2	9	3157	1283 ± 258	5.65	$1.1 \pm 0.6 \cdot 10^{16}$	$6.83 \cdot 10^{15}$
Augustine (Jan 17), 2006[4]	111	3.2	14	3637	1483 ± 298	6.06	$2.0 \pm 1.1 \cdot 10^{15}$	$9.37 \cdot 10^{15}$

[1] [*Yokoo and Ishihara*, 2007].

[2] [*Nairn*, 1976; *Nairn and Self*, 1978].

[3] [*Ripepe et al.*, 2013].

[4] [*Caplan-Auerbach et al.*, 2010].

D R A F T

D R A F T

Figure 1. Schematic of the Split-Hopkinson pressure bar test gun used as shock tube. Green, blue, and red lines indicate the filling, triggering, and expansion pads followed by the nitrogen during the different stages of the experiment, respectively.

Figure 2. Comparison of the theoretical and experimental non-dimensional shock wave speed versus position from the driven section end. Solid lines present the Mach number calculated using the strong shock wave theory, equation (4). Dashed lined symbols represent the experimental measurements of the shock wave speed (Mach number) versus relative position from the end of the driven section. The pressure wave becomes sonic when the wave speed drops to a Mach number of 1, at which point shock theory is no longer valid.

Figure 3. View of the Sakurajima vent before the eruption indicating the area of interest used to extract the wave. Video of Mt. Sakurajima's Showa crater taken at approximately 1:00 UTC on 30 January 2011. From the video recording, using similar technique than *Yokoo et al.* [2006] and *Yokoo and Ishihara* [2007], the shock wave position was stimated for every frame. Bottom: series of picture showing the shock wave displacement, highlighted by the red line, in time.

Figure 4. Symbols indicate the measured shock wave position versus time for the initial stage of the expansion of the shock wave as capture by a video camera at 30 fps shown in Figure 3. Image processing was performed using a similar method proposed by *Yokoo et al.* [2006] and *Yokoo and Ishihara* [2007]. Solid line indicates a linear fitting curve of the observations.

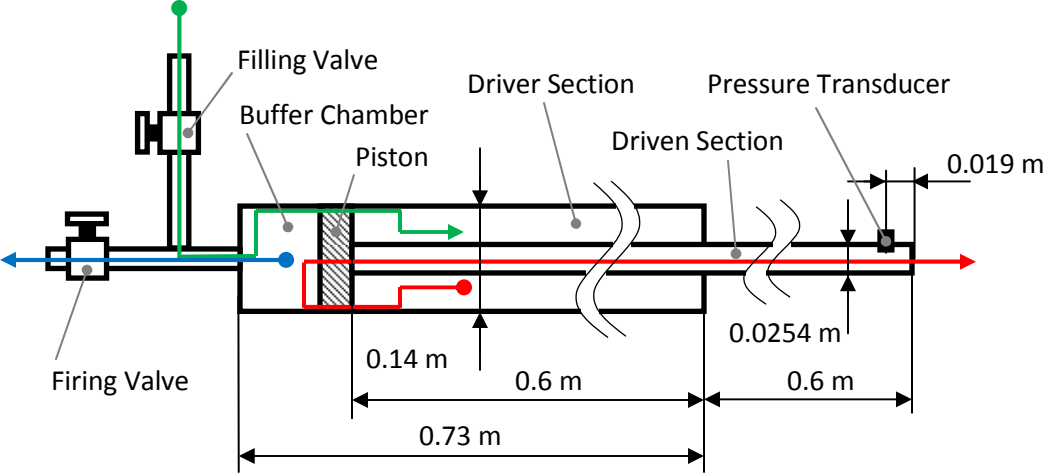
Filling Valve
Buffer Chamber
Piston
Driver Section
Driven Section
Pressure Transducer
0.019 m
Firing Valve
0.14 m
0.6 m
0.6 m
0.0254 m
0.73 m

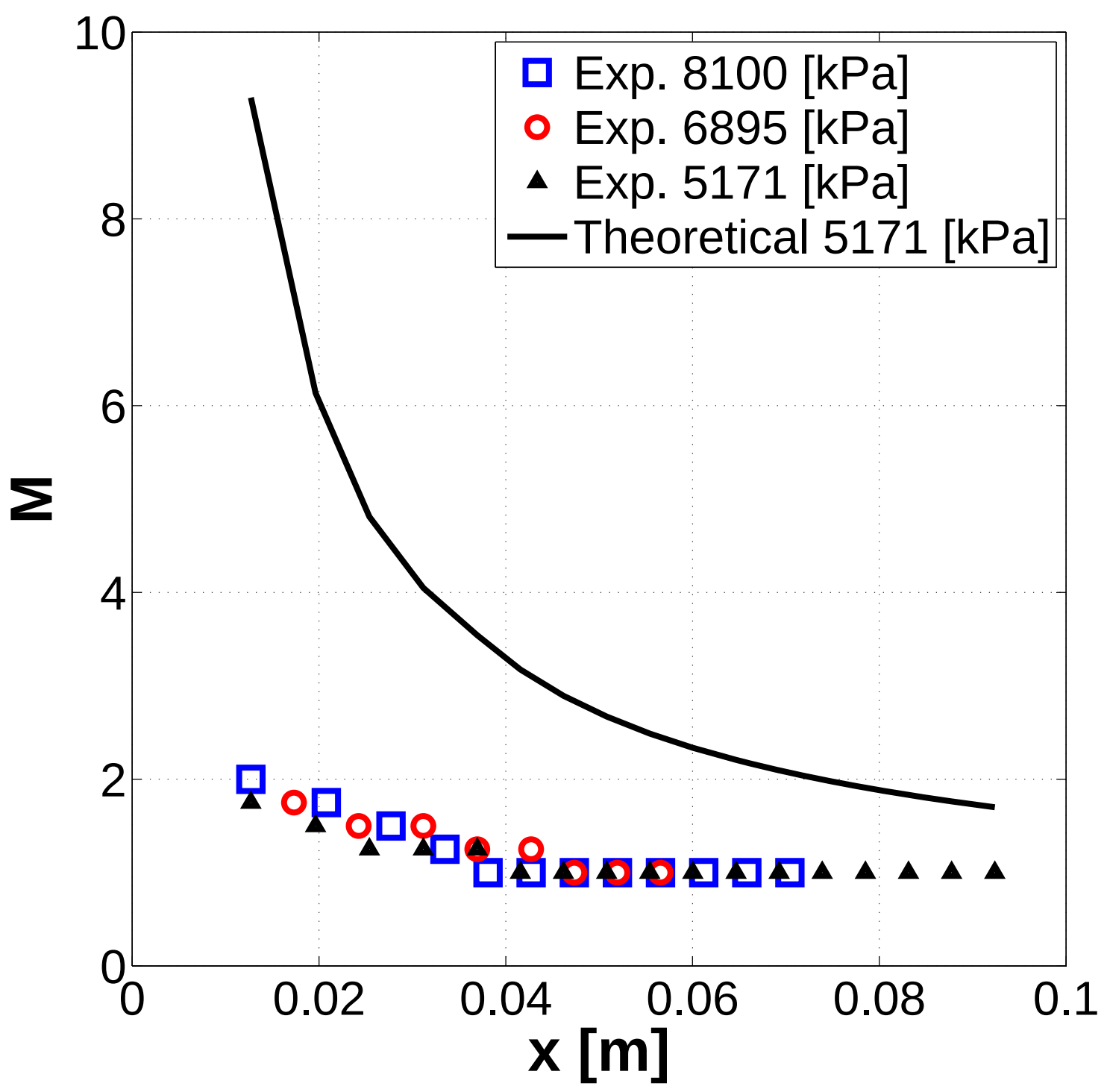
Exp. 8100 [kPa]
Exp. 6895 [kPa]
Exp. 5171 [kPa]
Theoretical 5171 [kPa]
M
x [m]
0
2
4
6
8
10
0
0.02
0.04
0.06
0.08
0.1

Area of Interest

0.0 s 0.033 s 0.066 s 0.1 s 0.133 s 0.166 s 0.2 s

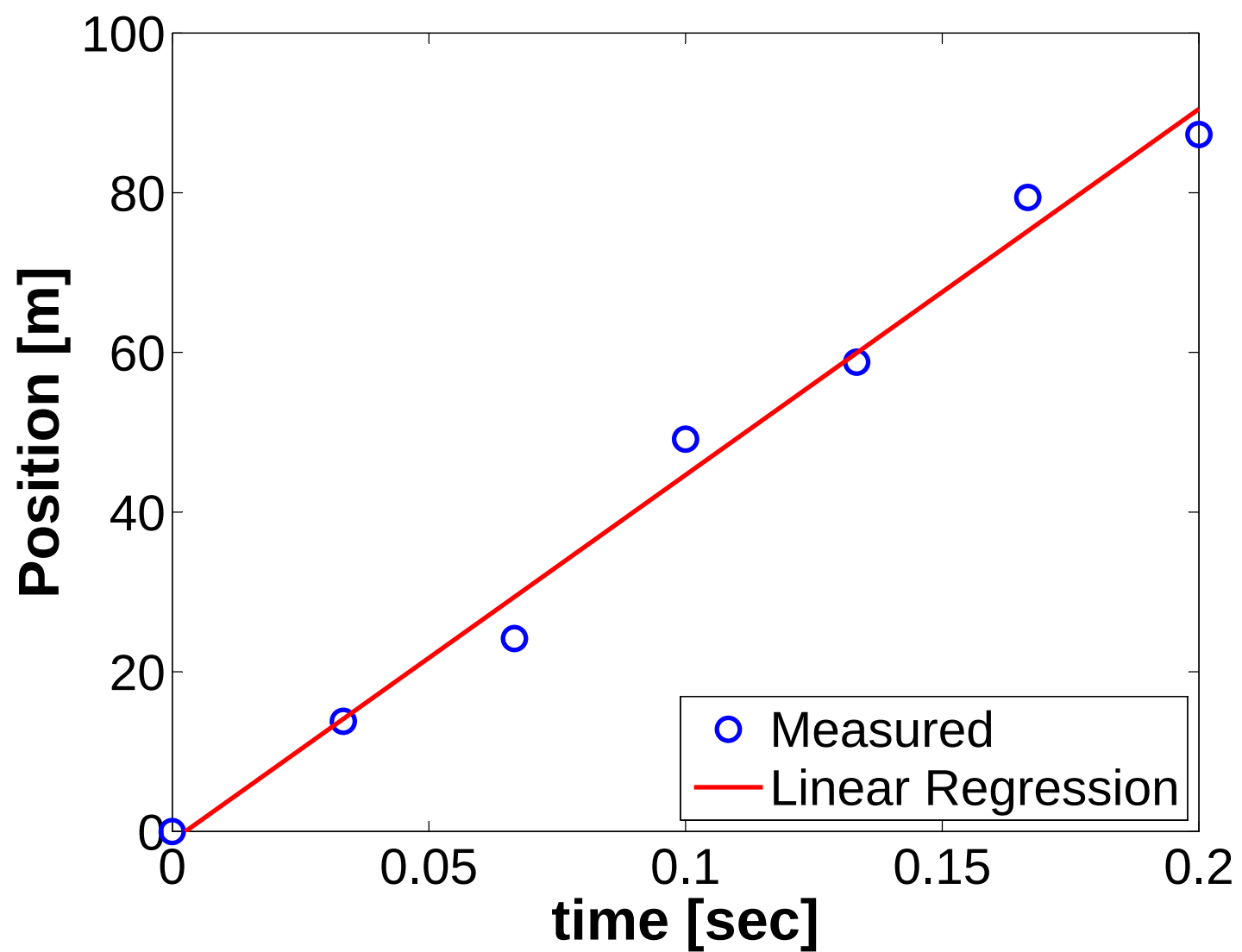
100
80
60
40
20
0
Position [m]
0
0.05
0.1
0.15
0.2
time [sec]
Measured
Linear Regression